



Calcium isotopic signatures of carbonatite and silicate metasomatism, melt percolation and crustal recycling in the lithospheric mantle

Dmitri A. Ionov^{a,b,*}, Yu-Han Qi^c, Jin-Ting Kang^{b,c}, Alexander V. Golovin^d,
Oleg B. Oleinikov^e, Wang Zheng^{f,g}, Ariel D. Anbar^f,
Zhao-Feng Zhang^b, Fang Huang^c

^a Géosciences Montpellier, Université de Montpellier, 34095 Montpellier, France

^b State Key Laboratory of Isotope Geochemistry, Guangzhou Institute of Geochemistry, Chinese Academy of Sciences, 510640 Guangzhou, China

^c CAS Key Laboratory of Crust-Mantle Materials and Environments, School of Earth and Space Sciences,

University of Science and Technology of China, Hefei 230026, China

^d Sobolev Institute of Geology and Mineralogy, Siberian Branch Russian Academy of Sciences, Koptyuga 3, Novosibirsk 630090, Russian Federation

^e Diamond and Precious Metal Geology Institute, Siberian Branch Russian Academy of Sciences, Lenina 39, Yakutsk 677007, Russian Federation

^f School of Earth and Space Exploration, Arizona State University, Tempe, AZ 85287, USA

^g Institute of Surface-Earth System Science, Tianjin University, Tianjin 300072, China

Received 10 July 2018; accepted in revised form 18 December 2018; Available online 26 December 2018

Abstract

Ca isotopes can be strongly fractionated at the Earth's surface and thus may be tracers of subducted carbonates and other Ca-rich surface materials in mantle rocks, magmas and fluids. However, the $\delta^{44/40}\text{Ca}$ range in the mantle and the scope of intra-mantle isotope fractionation are poorly constrained. We report Ca isotope analyses for 22 mantle xenoliths: four basalt-hosted refractory peridotites from Tariat in Mongolia and 18 samples from the Obnazhennaya (Obn) kimberlite on the NE Siberian craton. Obn peridotites are Paleoproterozoic to Archean melting residues metasomatised by carbonate-rich and/or silicate melts including unique xenoliths that contain texturally equilibrated carbonates. $\delta^{44/40}\text{Ca}$ in 15 Obn xenoliths shows limited variation (0.74–0.97‰) that overlaps the value ($0.94 \pm 0.05\%$) inferred for the bulk silicate Earth from data on fertile lherzolites, but is lower than $\delta^{44/40}\text{Ca}$ for non-metasomatised refractory peridotites from Mongolia ($1.10 \pm 0.03\%$). Bulk $\delta^{44/40}\text{Ca}$ in four Obn peridotites containing metasomatic carbonates ranges from $0.81 \pm 0.08\%$ to $0.83 \pm 0.06\%$, with similar values in acid-leachates and leaching residues, indicating isotopic equilibration of the carbonates with host rocks.

We infer that (a) metasomatism tends to decrease $\delta^{44/40}\text{Ca}$ values of the mantle, but its effects are usually limited ($\leq 0.3\%$); (b) Ca isotopes cannot distinguish “carbonatite” and “silicate” types of mantle metasomatism. The lowest $\delta^{44/40}\text{Ca}$ value (0.56‰) was obtained for a phlogopite-bearing Obn peridotite with a very high Ca/Al of 8 suggesting that the greatest metasomatism-induced Ca isotope shifts may be seen in rocks initially low in Ca that experienced significant Ca input leading to high Ca/Al. Two Obn peridotites, a dunite (melt channel material) and a veined spinel wehrlite, have high $\delta^{44/40}\text{Ca}$ values (1.22‰ and 1.38‰), which may be due to isotope fractionation by diffusion during silicate melt intrusion and percolation in

* Corresponding author at: Géosciences Montpellier, Université de Montpellier, 34095 Montpellier, France.
E-mail address: dmitri.ionov@gm.univ-montp2.fr (D.A. Ionov).

the host mantle. Overall, we find no evidence that recycling of crustal carbonates may greatly affect Ca isotope values in the global mantle or on a regional scale.

© 2018 Elsevier Ltd. All rights reserved.

Keywords: Ca isotopes; Isotope fractionation; Lithospheric mantle; Carbonate; Metasomatism; Crustal recycling

1. INTRODUCTION

Two most abundant Ca isotopes, ^{40}Ca (96.94%) and ^{44}Ca (2.09%), have a mass difference of about 10% (Heuser et al., 2002) and thus can experience significant fractionation at low temperatures near the Earth's surface. The Ca isotope compositions, expressed as $\delta^{44/40}\text{Ca}$ relative to the NIST SRM 915a reference material, range by up to several permil in Ca-rich sedimentary and other rocks formed or altered near the surface (Amini et al., 2009; Fantle and Tipper, 2014; Feng et al., 2016; Blättler and Higgins, 2017). In contrast, high temperature equilibrium isotope fractionation in the mantle should be at least an order of magnitude lower (e.g. Huang et al., 2010; Wang et al., 2017; Zhu et al., 2018). This difference may make it possible to use Ca isotopes to trace recycling of Ca-rich surface materials because mantle rocks contaminated by surface materials may have unusual isotope ratios. Hence, Ca isotopes may shed more light on the long-lasting debate on the role of crustal components in the mantle (e.g. Xu, 2002) along with other non-conventional stable isotopes (e.g. Huang et al., 2011; Wang et al., 2016). Ca isotopes are particularly promising to explore the role of subducted Ca-rich sediments in the sources of mantle metasomatism and mantle-derived magmas (e.g. Zeng et al., 2010; Huang S. et al., 2011; Chen et al., 2018), and in carbon cycling (e.g. Tappe et al., 2017).

The application of Ca isotopes to these topics necessitates a good knowledge of, first, the range of Ca isotope compositions in pristine mantle rocks that contain no crustal additions, and second, the extent of intra-mantle isotope differentiation by melting and metasomatism including non-equilibrium processes like diffusion (e.g. Zhao et al., 2017) and inter-mineral fractionation (Huang et al., 2010; Kang et al., 2016; Wang et al., 2017). Recently, Kang et al. (2017) reported Ca isotope compositions for mantle peridotites ranging from fertile lherzolites to harzburgites, and constrained the Ca isotope composition of the bulk silicate Earth (BSE) and pristine melting residues. They also found that $\delta^{44/40}\text{Ca}$ in metasomatized peridotites spans a range from the BSE to considerably lower values.

Here we report $\delta^{44/40}\text{Ca}$ for a suite of strongly metasomatized, Ca-enriched mantle rocks to better define the Ca isotope range in the lithospheric mantle, primarily to constrain the role of metasomatism by carbonate-rich and silicate melts. We provide whole rock (WR) data for 16 peridotite and two pyroxenite xenoliths from the Obnazhennaya (Obn) kimberlite in the NE Siberian craton (Ionov et al., 2015; Ionov et al., 2018b) as well as for acid leachates and leaching residues of three Obn peridotites that contain metasomatic carbonate. We also report WR data for four refractory non-metasomatized peridotite xenoliths from

Tariat in Mongolia (Ionov and Hofmann, 2007) to better define the Ca isotope range in pristine melting residues.

2. LOCALITIES AND SAMPLES

2.1. Obnazhennaya and its mantle xenoliths

The ~160 Ma Obnazhennaya kimberlite (70°15'N, 121°35'E) is located in the NE Siberian craton (Fig. 1). It is one of only two kimberlites in Siberia that contain peridotite xenoliths sufficiently large and fresh for WR petrogeochemical studies. Re-Os isotope data suggest that their sources experienced partial melting at ~1.9 and 2.8 Gy ago (Ionov et al., 2015, 2018a). Petrographic and chemical data (Ionov et al., 2018b/and references therein) suggest that the Obn xenolith suite is unusual for cratons, with common peridotites rich in clinopyroxene (cpx) and garnet but low in orthopyroxene (opx), no sheared rocks, and low P-T values suggesting a very thin mantle lithosphere (≤ 100 km). Some samples contain alteration products (mainly serpentine at grain boundaries and veins in olivine), but they are less common than in most cratonic suites elsewhere.

The Obn peridotites have protogranular to mosaic-equigranular microstructures and are grouped into four series (Table 1): (1) low-cpx spinel harzburgites and dunites;

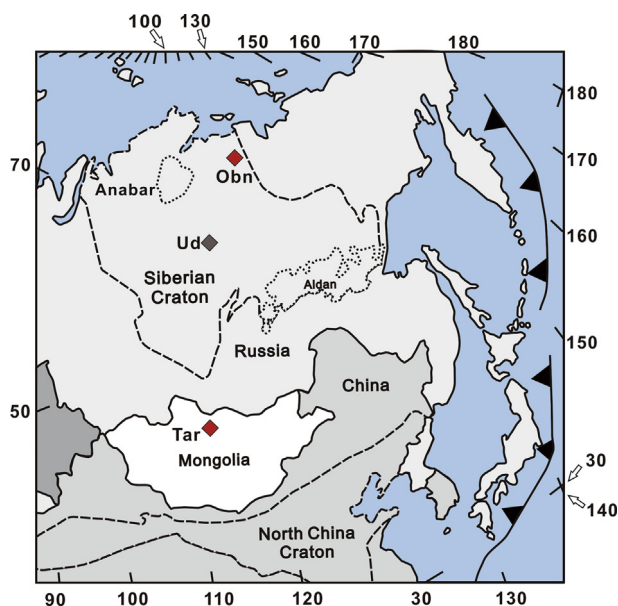


Fig. 1. Locality map for the Obnazhennaya (Obn) and Udachnaya (Ud) kimberlite pipes on the Siberian craton, and the Cenozoic Tariat (Tar) volcanic field in central Mongolia.

Table 1
Summary of essential data on xenoliths.

Sa. No.	Rock type	$\delta^{44/40}\text{Ca}$	T°C	P, GPa	Whole-rock composition, wt.%				Ol Mg#	Modal composition, %							
		SRM 915a			Ca-opx	Al-opx	Al ₂ O ₃	CaO		Ca/Al	Mg#	Ol	Opx	Cpx	Sp	Gar	Phl
<i>Low-Ca-Al dunites and harzburgites</i>																	
Obn 59-13	Sp Dunite	1.22	n.a.	n.a.	0.14	0.38	3.7	0.915	0.916	98.2	–	1.5	0.4	–	–	–	–
Obn 60-13	Sp-rich Dunite	0.96	n.a.	n.a.	0.93	0.63	0.9	0.888	0.892	94.4	–	2.2	3.3	–	–	–	–
Obn 69-13	Sp Hz	0.90	923	/1.5/	0.76	0.33	0.6	0.918	0.921	74.8	23.8	0.7	0.7	–	–	–	–
<i>Phl-bearing, mainly carbonate bearing, Ca-rich peridotites with low to moderate Al</i>																	
Obn 08-13	Gar-Sp-Phl Hz	0.85	729	2.1	1.20	2.77	3.1	0.919	0.921	69.9	20.4	0.8	0.5	2.3	1.6	4.4	–
Obn 22-13	Sp Hz	0.81	1027	/1.5/	1.82	2.20	1.6	0.917	0.920	76.1	15.8	1.9	2.6	–	0.5	3.1	–
Obn 24-13	Sp-Phl Lh	0.56	784	/1.5/	0.41	2.44	8.0	0.918	0.920	84.2	6.6	3.6	0.1	–	2.4	3.1 ^a	–
Obn 39-13	Gar-Sp Hz	0.81	711	1.6	1.90	3.17	2.3	0.918	0.920	66.4	20.7	2.1	1.3	4.0	1.1	4.5	–
Obn 53-13	Gar-Sp-Phl Hz	0.74	767	2.6	1.42	3.22	3.1	0.919	0.924	75.7	12.0	0.5	1.7	2.9	1.8	5.4	–
<i>Ca-rich peridotites with low to moderate Al</i>																	
Obn 12-13	Sp Lh-Wh	0.88	1047	/1.5/	1.63	2.44	2.0	0.920	0.921	84.0	2.6	10.7	2.6	–	–	–	–
Obn 37-13	Sp Lh-Wh	0.78	685	/1.5/	0.57	2.48	5.9	0.915	0.918	85.2	3.9	10.5	0.4	–	–	–	–
Obn 68-13	Sp Wh	1.38	891	/1.5/	0.88	2.94	4.5	0.909	0.912	84.0	2.5	12.4	1.2	–	–	–	–
O-1017	Sp Lh	0.77	706	/1.5/	1.10	2.50	3.1	0.917	0.923	74.8	13.0	11.2	1.0	–	–	–	–
O-1061	Gar-Sp Hz	0.81	716	/1.5/	0.82	1.95	3.2	0.916	0.919	87.7	2.6	4.2	1.3	4.2	–	–	–
<i>Ca, Al-rich lherzolites</i>																	
Obn 06-13	Sp Lh	0.97	668	/1.5/	3.25	4.86	2.0	0.924	0.924	68.7	5.7	21.7	4.0	–	–	–	–
Obn 21-13	Gar-Sp Lh	0.97	698	2.0	7.98	5.49	0.9	0.900	0.922	44.7	7.0	17.4	1.1	29.8	–	–	–
O-47	Sp Lh	0.80	n.a.	n.a.	2.66	3.76	1.9	0.909	0.908	61.8	22.0	16.2	n.a.	–	–	–	–
<i>Garnet and plagioclase pyroxenites</i>																	
Obn 58-13	Sp-Pl Wbst vein	0.74	n.a.	n.a.	11.08	3.22	0.4	0.919	–	–	28.9	59.1	7.6	–	–	–	4.5
O-1080	Ol-Gar-Sp Wbst	0.93	729	2.1	7.18	8.02	1.5	0.909	0.922	30.1	12.6	38.1	1.3	17.9	–	–	–
<i>Refractory Tariat peridotites</i>																	
Mo4399- 23	Sp Hz	1.08	876	/1.5/	0.88	0.78	1.2	0.912	0.913	n.a.	n.a.	n.a.	n.a.	n.a.	n.a.	n.a.	n.a.
Mo-92	Low-cpx Sp Lh	0.96	898	/1.5/	2.14	1.65	1.0	0.912	0.913	n.a.	n.a.	n.a.	n.a.	n.a.	n.a.	n.a.	n.a.
Mo-94a	Sp Hz	1.12	886	/1.5/	0.96	0.76	1.1	0.910	0.911	n.a.	n.a.	n.a.	n.a.	n.a.	n.a.	n.a.	n.a.
Mo-95	Low-cpx Sp Lh	0.99	868	/1.5/	1.54	1.38	1.2	0.908	0.909	n.a.	n.a.	n.a.	n.a.	n.a.	n.a.	n.a.	n.a.

See Table 2 for details of Ca isotope data (reproducibility, accuracy, analyses of reference samples). Value for Obn 8-13 is an average of two full duplicates.

Data on the samples are from Ionov et al. (2018b). Sample 58-13 is a vein in a harzburgite.

Ol, olivine; Opx, orthopyroxene; Cpx, clinopyroxene; Sp, spinel; Gar, garnet; Carb, carbonate (calcite); Phl, phlogopite; Pl, plagioclase.

Lh, lherzolite; Hz, harzburgite; Wh, wehrlite; Wbst, websterite; n.a., not available; –, absent.

See Ionov et al. (2018b) for opx-based methods used to obtain equilibration temperatures (T) and pressures (P); P = 1.5 GPa is assumed for spinel peridotites.

Modal estimates obtained by least squares method from whole-rock and mineral analyses, and normalized to 100%.

^a Modal carbonate in sample 24-13 is an estimate for a hypothetical calcite component that could react with opx to yield metasomatic Cpx-Spl ± Phl pockets.

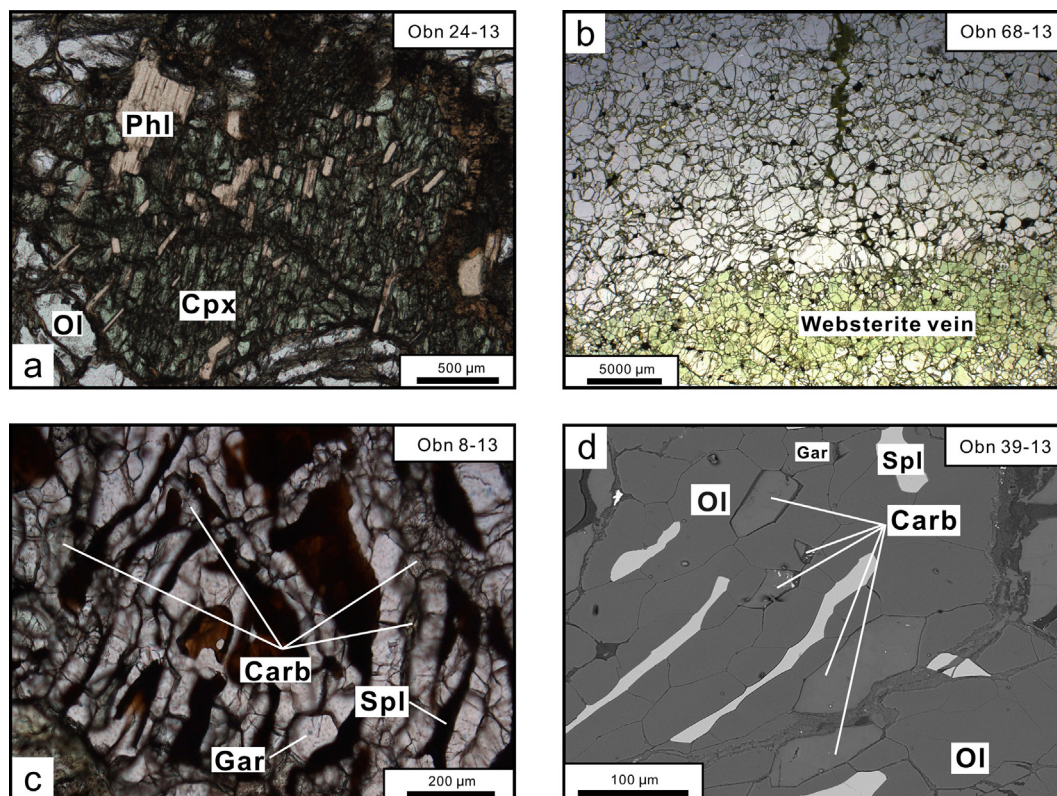


Fig. 2. Photomicrographs in transmitted plane-polarized light (a–c), and a back-scattered electron (BSE) image (d) of Obnazhennaya peridotite xenoliths. Abbreviations: Carb, carbonate; Cpx, clinopyroxene; Phl, phlogopite; Spl, spinel; Gar, garnet; Ol, olivine. (a) Pocket of Cpx, Phl and Cr-spinel in Obn 24-13, likely formed by reaction of carbonate-rich media with orthopyroxene. (b) Websterite vein in fine-grained, mosaic, spinel peridotite Obn 68-13; thin dark veinlet in the peridotite is chlorite, a Ca-free alteration mineral. (c) Carb-Gar-Ol-Spl pocket similar to that shown in detail in d. (d) Carbonate (Mg-Fe-Mn-bearing calcite) texturally equilibrated (straight grain boundaries) with garnet and olivine.

(2) phlogopite- and carbonate-bearing, Ca-rich rocks with low to moderate Al; (3) peridotites with low to moderate Al, rich in Ca and cpx; (4) Ca-Al-rich lherzolites rich in pyroxenes \pm garnet. They are distinguished from typical cratonic xenolith suites by the rarity of harzburgites and by gradual modal variations of olivine, pyroxenes and garnet between peridotites and pyroxenites. In some of these rocks opx is replaced with late-stage cpx \pm phlogopite (Fig. 2a). Three peridotites contain pockets of carbonate (Mn-Mg-bearing calcite) texturally equilibrated with garnet and olivine (Fig. 2c and d); these rocks are unique because peridotite xenoliths containing carbonates of mantle origin are extremely rare (e.g., Ionov et al., 1993). Pyroxenites (websterites) occur as discrete xenoliths (O-1080) and veins in peridotites (Obn 58-13 and 68-13; Fig. 2b).

The majority of the Obn xenoliths have low Al_2O_3 (≤ 1.9 wt.%) and high MgO ($>42\%$), consistent with an origin as residues of high-degree partial melting because these oxides are considered to be robust melt extraction indices, and because they plot on the Al-Mg trend defined by experimental and natural (Tariat) melting residues (Fig. 3a). Yet the Obn xenoliths also show petrographic and chemical

features that cannot be explained by melt extraction alone, in particular anomalously high CaO at given Al_2O_3 (Fig. 3b). As a result, the Ca/Al ratios of nearly all Obn peridotites in this study are much higher than in the primitive mantle (McDonough and Sun, 1995) and in residual mantle peridotites (Palme and Nickel, 1985; Ionov and Hofmann, 2007) (1.6–8.0 vs. 1.0–1.5; Fig. 3c). These and other data suggest that the Obn xenoliths initially formed as refractory melting residues, but were reworked by silicate and/or carbonatite metasomatism with significant Ca input. The Ca-Al-rich rocks formed by reaction and mingling with large amounts of silicate melts. The three Series 1 peridotites low in both Ca and Al are melt-channel materials (Ionov et al., 2018b).

Another four peridotite xenoliths are from late Cenozoic (~ 0.5 Ma) alkali basaltic breccia at Shavaryn-Tsaram in the Tariat district of central Mongolia (Ionov, 2007) within the Central Asian orogenic belt. The samples are cpx-poor lherzolites or cpx-bearing spinel harzburgites with modal and major oxide compositions typical for refractory melting residues, and no evidence for metasomatism (Ionov and Hofmann, 2007). Their Al_2O_3 range (1.0–2.1 wt.%; Table 1)

is similar to that for the Obn peridotites, but the Tariat peridotites show no Ca enrichments and no anomalous Ca/Al ratios (Fig. 3).

2.2. Sample selection and treatment

The samples (aliquots of those reported by Ionov et al., 2018b; Ionov and Hofmann, 2007) are listed in Table 1 that provides a summary of essential petrologic and chemical

data. The xenoliths are 10–30 cm in size. Their rinds were removed by sawing. Slabs of fresh material from xenolith cores were inspected to make sure they contain no host lava, veins or modal gradations. A large amount of fresh material (normally >100 g) was taken to provide representative WR samples and crushed to <5–10 mm in a steel jaw crusher carefully cleaned to avoid cross-contamination. Splits of crushed material (50–100 g) were ground to fine powder in agate.

Three carbonate-bearing Obn peridotites (8-13, 22-13 and 39-13) were acid-leached to dissolve metasomatic calcite and analyze the resulting solution and the residue after leaching. Aliquots of crushed (≤ 2 mm) rocks were treated with 5 ml of 10% HNO_3 for 2 min at room temperature, which produced CO_2 bubbles for less than a minute. The solution was extracted, the residue washed with 2 ml milli-Q water four times, and the wash water was added to the acid-leach solution for analysis. The residues were dissolved using the same procedure as for WR powders (described below). Previous work showed that leaching of silicate minerals (including phlogopite and amphibole) and glass from mantle xenoliths with diluted cold HNO_3 for a few minutes does not destroy these phases nor affect their surfaces (e.g., Ionov and Hofmann, 1995; Ionov et al., 1993).

3. ANALYTICAL PROCEDURES AND DATA QUALITY

Sample dissolution, chemical purification and mass spectrometric analysis of Ca were done at Arizona State University (ASU) following procedures defined by Romaniello et al. (2015). Briefly, 10–60 mg of rock powder was digested using a mixture of concentrated HF and HNO_3 (5:1) in a 7 mL Savillex™ PFA beaker on hot plate at 110 °C for 2–3 days. After the digestion, the samples were dried at 80 °C and refluxed with 6 M (mol/L) HCl several times to remove precipitated CaF_2 until completely

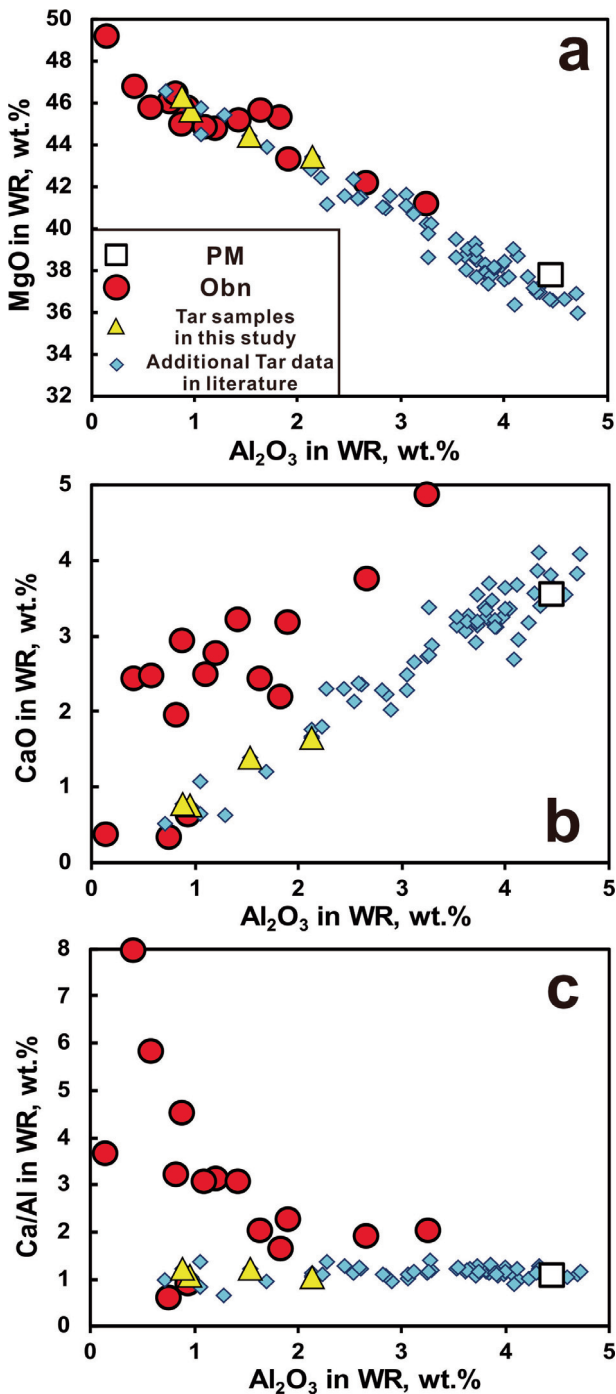


Fig. 3. Co-variation plots of MgO (a), CaO (b) and Ca/Al (c) vs. Al_2O_3 (wt.%) in whole-rock (WR) peridotite xenoliths from Obnazhennaya (Obn, large circles; Obn 21-13 with ~ 8 wt.% Al_2O_3 is beyond the scale) and Tariat (“Tar”, triangles). Also shown (small rhombs) are additional Tariat samples from the literature (Ionov and Hofmann, 2007; Ionov, 2007), which were not analyzed for Ca isotopes, and primitive mantle (PM) after McDonough and Sun (1995); PM is a term used in studies of chemical composition of mantle xenoliths, which is essentially equivalent to BSE commonly used in isotope studies. The Obn peridotites plot close to the melt extraction trend defined by the literature data for Tariat xenoliths on the Al–Mg diagram (a); this is because both Al and Mg are robust melt extraction indices and are little affected by metasomatism. In contrast, the majority of the Obn peridotites have much higher CaO and Ca/Al due to post-melting Ca enrichments. The highest Ca/Al ratios are in low- Al_2O_3 (<1.5 wt.%) rocks, i.e. residues of high degrees of melt extraction initially strongly depleted in Ca, for which the metasomatic input dominates the WR Ca budget.

dissolved, then evaporated to dryness. The dried material was dissolved in 2 M HNO₃ for column chemistry.

Separation of Ca from sample matrix was performed automatically using the prepFAST MC (ESI, Omaha, NE, USA) and the supplied 1 mL Sr-Ca column (part number CF-MC-SrCa-1000) following the method of Romaniello et al. (2015). Elution uses 2 M HNO₃ + 1 wt. % H₂O₂ to remove most major and trace matrix elements. Sr is eluted in 6 M HNO₃ and Ca with 12 M HNO₃. In the final step, 10 mL of 1 M HF is used to remove all remaining elements from the resin (REE, Hf, Cd and U). The Ca yield of the column chemistry, calculated by comparing the amount of Ca before and after the column procedure, ranged from 90% to 93%. Romaniello et al. (2015) found no detectable Ca isotope fractionation at Ca yields as low as 75%. The concentrations of Ca and other elements were measured using an ICAP-Q quadrupole inductively-coupled plasma mass spectrometer (ICP-MS: Thermo Scientific, Bremen, Germany) at ASU following the method of Romaniello et al. (2015).

Calcium isotope compositions were measured on a Neptune multi-collector (MC) ICP-MS (Thermo Scientific, Bremen, Germany) at ASU equipped with a Jet sample cone, an H-skimmer cone, and an Apex-Q desolvating nebulizer (ESI, Omaha, NE, USA). Measurements were done using the double spike method with sample-standard bracketing. The Ca double spike was prepared from two isotopically enriched CaCO₃ powders (Isoflex USA) containing ⁴³Ca (62.20 atom%) and ⁴⁶Ca (15.90 atom%), respectively. The isotope compositions of the double spike and the in-house natural isotope standard (“ICP1” NIST 10,000 ppm ICP Ca standard, lot #X-10-39A) were calibrated using MC-ICP-MS. The double-spike solution was added as 2% of the total Ca concentration in samples ≥24 h before the isotope analysis to allow full spike-sample equilibration.

The samples and standards were measured in high-resolution mode with a mass resolution of ≥8000 (measured as M/ΔM, where ΔM is the mass difference at 5% and 95% peak height). Optimized instrument operating parameters were: sample gas, 0.9 L min⁻¹; auxiliary gas, 0.9 L min⁻¹; cooling gas, 14.50 L min⁻¹, and N₂ of 2–5 mL min⁻¹. Ca samples were introduced at a concentration of 3 μg/g and flow rate of 200 mL min⁻¹ yielding a sensitivity of ~3.3 V ⁴⁴Ca⁺ per μg/g Ca. Faraday cups were positioned to measure ⁴²Ca⁺, ⁴³Ca⁺, ⁴⁴Ca⁺, ⁴⁵Sc⁺, ⁴⁶Ca⁺, ⁴⁷Ti⁺, and ⁴⁸Ca⁺. ⁴⁵Sc was measured to align the uninterfered low-mass shoulder of the Ca and Ti isotopes with its peak center. Once aligned, the center cup was set to measure an optimal position on the uninterfered low-mass peak shoulder of Ca isotopes. ⁴⁷Ti was monitored to correct for the isobaric interference of ⁴⁸Ti on ⁴⁸Ca. Doubly charged Sr²⁺, which is a common isobaric interference for Ca isotopes, was monitored for all samples and standards using a sub-configuration of Faraday cups. Details of the cup configuration and interference corrections are given in Romaniello et al. (2015). Double-spiked Ca samples were run in sequence with every two samples bracketed by the equivalently spiked ICP1 in-house standard. Mass bias and corrected isotopic ratios were calculated using the Newton-Rhapon procedure (Albarede and Beard, 2004).

Three purified and double-spiked secondary Ca standards (international reference materials NIST SRM 915a, NIST SRM 915b, and IAPSO: <http://www.ciaaw.org/calcium-references.htm>) were measured every 10–14 samples in each analytical session to check if the method consistently produces accurate and precise values. NIST SRM915a and SRM915b are carbonate reference materials, and IAPSO is seawater; all secondary standards were purified using the same procedure as the samples. The Ca isotope ratios are calculated in delta notation ($\delta^{44/42}\text{Ca}_{\text{SRM915a}}$, $\delta^{44/42}\text{Ca} (\text{‰}) = [({}^{44}\text{Ca}/{}^{42}\text{Ca})_{\text{sample}} / ({}^{44}\text{Ca}/{}^{42}\text{Ca})_{\text{NIST SRM 915a}} - 1]$). Final data are reported as $\delta^{44/40}\text{Ca}_{\text{SRM915a}}$ ($\delta^{44/40}\text{Ca} (\text{‰}) = [({}^{44}\text{Ca}/{}^{40}\text{Ca})_{\text{sample}} / ({}^{44}\text{Ca}/{}^{40}\text{Ca})_{\text{NIST SRM 915a}} - 1]$) obtained by multiplying $\delta^{44/42}\text{Ca}_{\text{SRM915a}}$ by a scaling factor of 2.049 based on kinetic mass dependent fractionation (Young et al., 2002) (Table 2).

All samples were measured at least 3 times; the analytical error is reported as 2 standard deviations (2SD) of replicate measurements. Long-term external precision (2SD of $\delta^{44/42}\text{Ca}$ in SRM915a) during this study was 0.08‰ (n = 24), and the precision for $\delta^{44/40}\text{Ca}$ can be propagated as $0.08 \times 2.049 \approx \pm 0.16\text{‰}$. Mean $\delta^{44/40}\text{Ca}$ values (relative to SRM915a) for reference samples run in the same session (Table 2) are: SRM915a, $0.00 \pm 0.16\text{‰}$ (n = 24); SRM915b, $0.70 \pm 0.16\text{‰}$ (n = 20); IAPSO Seawater, $1.82 \pm 0.16\text{‰}$ (n = 17); BHVO-2, $0.82 \pm 0.10\text{‰}$ (n = 3); PCC-1, $1.29 \pm 0.02\text{‰}$ (n = 3). These values agree with data in the literature, for example He et al. (2016) reported $0.79 \pm 0.09\text{‰}$ (n = 7) for BHVO-2 and Liu et al. (2017) reported $1.15 \pm 0.09\text{‰}$ (n = 7) for peridotite PCC-1 (see also Valdes et al., 2014; Feng et al., 2016; Amsellem et al., 2017) confirming the robustness of our analytical procedure. In addition, full duplicates of sample Obn 8-13 obtained by digestion of two batches of powder reproduced within the analytical error (Table 2).

4. RESULTS

4.1. Ca isotopes in whole-rock xenoliths

The $\delta^{44/40}\text{Ca}$ values in the WR xenoliths from the Obn suite (Table 2) range from 0.56 to 1.38‰, but the range is much more narrow (0.74–0.97‰) for 15 out of 18 samples analyzed (Fig. 4). These 15 samples are mainly harzburgites, but also include spinel and garnet lherzolites, wehrlites and pyroxenites, i.e. all main rock types in the Obn suite (Ionov et al., 2018b). The three outliers are xenoliths with unusual rock types or major oxide compositions. The highest $\delta^{44/40}\text{Ca}$ ($1.38 \pm 0.04\text{‰}$) is in Obn 68-13, the only peridotite sample in the suite taken close to contact with a pyroxenite vein (Fig. 2b). The other sample with high $\delta^{44/40}\text{Ca}$ ($1.22 \pm 0.07\text{‰}$) is a spinel dunite (melt channel material consisting of olivine and accessory chromite) with the lowest Al₂O₃ (0.14 wt.%) among our samples. The lowest $\delta^{44/40}\text{Ca}$ value ($0.56 \pm 0.03\text{‰}$) is for peridotite Obn 24-13, in which coarse opx is replaced with fine-grained pockets of cpx, phlogopite and chromite (Fig. 2a).

Four off-craton peridotite xenoliths from Tariat in Mongolia (harzburgites to low-cpx lherzolites) have $\delta^{44/40}\text{Ca}$

Table 2
Whole-rock Ca isotope compositions of xenoliths and reference samples.

Sa. No.	Rock type	$\delta^{44/42}\text{Ca}$ relative to ICPI	2SD	$\delta^{44/40}\text{Ca}$ relative to SRM 915a	$\delta^{44/40}\text{Ca}$ relative to SRM 915b	2SD	n
<i>Obn low Ca-Al dunite and harzburgite</i>							
Obn-59/13	Sp Dunite	0.25	0.03	1.22	0.52	0.07	3
Obn-60/13	Sp-rich Dunite	0.12	0.02	0.96	0.26	0.04	3
Obn-69/13	Sp Hz	0.09	0.09	0.90	0.20	0.18	3
<i>Obn Phl-bearing, mainly carbonate bearing, Ca-rich peridotites with low to moderate Al</i>							
Obn-8/13	Gar-Spl-Phl Hz	0.08	0.02	0.88	0.18	0.04	3
^a Obn-8/13		0.06	0.06	0.83	0.13	0.12	3
R							
^b Obn-22/13	Sp Hz, vermic.	0.04	0.06	0.81	0.11	0.12	3
Obn-24/13	Sp-Phl Lh	−0.08	0.01	0.56	−0.14	0.03	3
^b Obn-39/13	Gar-Sp Hz	0.05	0.04	0.81	0.11	0.08	3
Obn-53/13	Gar-Sp-Phl Hz	0.01	0.04	0.74	0.04	0.09	3
<i>Obn Ca-rich peridotites with low to moderate Al</i>							
Obn-12/13	Sp Lh-Wh, vermic	0.08	0.05	0.88	0.18	0.11	3
Obn-37/13	Sp Lh-Wh	0.03	0.06	0.78	0.08	0.13	3
Obn-68/13	Sp Wh	0.32	0.02	1.38	0.68	0.04	3
O-1017	Sp Lh	0.02	0.04	0.77	0.07	0.07	3
O-1061	Gar-Sp Hz vermic	0.04	0.07	0.81	0.11	0.14	3
<i>Obn Ca, Al-rich lherzolites</i>							
Obn-6/13	Sp Lh, protogran	0.12	0.01	0.97	0.27	0.02	3
Obn-21/13	Gar-Sp Lh	0.12	0.03	0.97	0.27	0.06	3
O-47	Sp Lh	0.04	0.07	0.80	0.10	0.14	3
<i>Obn garnet and plagioclase pyroxenites</i>							
Obn-58/13	Sp-Pl Wbst vein	0.01	0.01	0.74	0.04	0.03	3
O-1080	Ol-Gar-Sp Wbst	0.11	0.07	0.93	0.23	0.14	3
<i>Refractory Tariat peridotites</i>							
Mo4399-23	Sp Hz	0.18	0.01	1.08	0.38	0.03	3
Mo-92	Low-cpx Sp Lh	0.12	0.02	0.96	0.26	0.05	3
Mo-94a	Sp Hz	0.20	0.01	1.12	0.42	0.03	3
Mo-95	Low-cpx Sp Lh	0.13	0.02	0.99	0.29	0.05	3
<i>International reference samples</i>							
SRM 915a	Carbonate	−0.35	0.08	0	−0.70	0.16	24
SRM 915b	Carbonate	−0.01	0.08	0.70	0	0.16	20
IAPSO	Seawater	0.54	0.08	1.82	1.13	0.16	17
PCC-1	Sp Lh	0.28	0.01	1.29	0.59	0.02	3
BHVO-2	Basalt	0.05	0.05	0.82	0.12	0.1	3

ICPI, in-house Ca isotope standard (see text). See Table 1 for other abbreviations.

n, number of repeated measurements of the same solution.

^a R denotes full procedural replicated sample.

^b Calculated based on the analyses of residue and leachate given in Table 3.

values from 0.96 to 1.12‰. Their range overlaps the highest $\delta^{44/40}\text{Ca}$ values found in four out of 15 “conventional” Obn xenoliths (0.96–0.97‰), but is considerably higher than $\delta^{44/40}\text{Ca}$ in the remaining 11 Obn samples (0.74–0.88‰) (Fig. 4).

4.2. Ca isotope data from acid-leaching experiments

Leaching by diluted HNO_3 done on crushed (but not ground) aliquots of three xenoliths should dissolve metasomatic calcite, but leave intact the silicate and oxide

minerals. For one sample (Obn 8-13, Fig. 2c) the WR powder was analyzed in duplicate. The additional $\delta^{44/40}\text{Ca}$ values determined for the leachate and residue, as well as bulk $\delta^{44/40}\text{Ca}$ values calculated using the Ca proportions in the leachate and residue for each sample, are given in Table 3.

All four analyses obtained on sample Obn 8-13 are within analytical uncertainty, with $\delta^{44/40}\text{Ca}$ values of $0.88 \pm 0.04\text{‰}$ and $0.83 \pm 0.12\text{‰}$ for the WR duplicates, $0.82 \pm 0.01\text{‰}$ for the leachate and $0.84 \pm 0.06\text{‰}$ in the residue. The differences between the leachate and residue for two other samples are insignificant as well: $0.84 \pm 0.04\text{‰}$ for

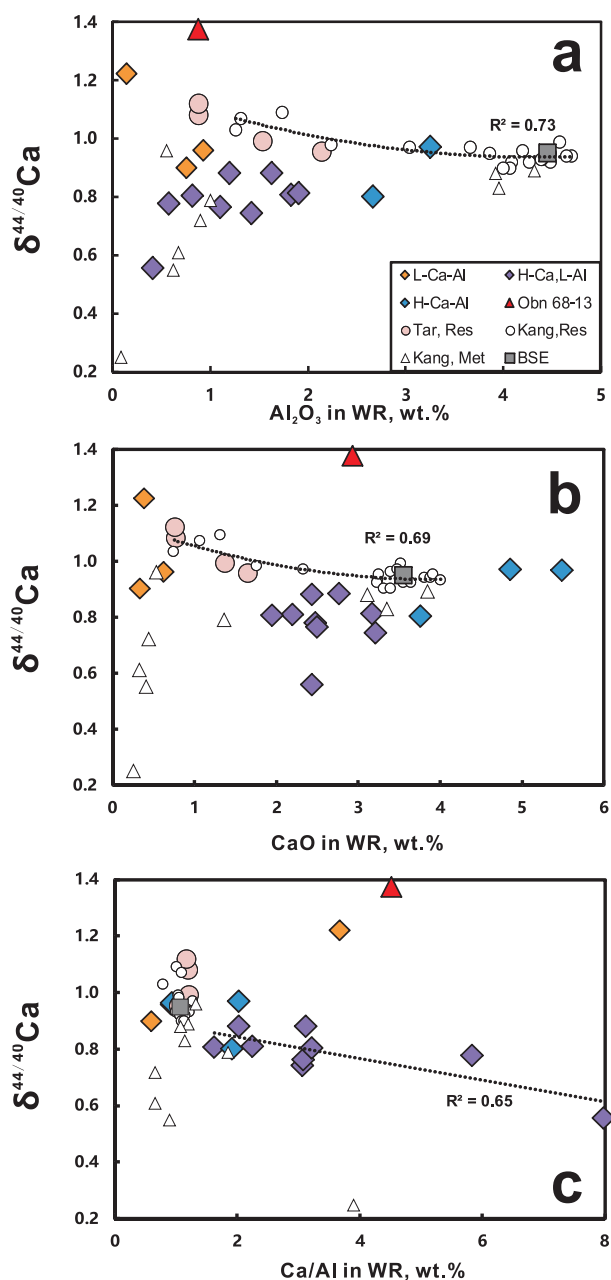


Fig. 4. Co-variation plots of $\delta^{44/40}\text{Ca}$ vs. (a) Al_2O_3 , (b) CaO and (c) Ca/Al (wt.%) in whole-rock peridotite xenoliths from Obnazhenaya and Tariat. Large filled symbols, data from this study (circles, non-metasomatized melt-depleted Tariat peridotites; rhombs, metasomatized Obn xenoliths; triangle, Obn peridotite next to a vein); small empty symbols, data from Kang et al. (2017) for residual (KangRes, circles) and metasomatized (KangMet) peridotite xenoliths. Abbreviations: L, low (<2 wt.%); H, high; BSE, bulk silicate Earth (primitive mantle). Also shown are co-variation trends (best-fit lines: exponential in a-b and linear in c) and coefficients (R^2) for residual, non-metasomatized Tariat peridotites from this study combined with those from Kang et al. (2017). The metasomatized peridotites tend to have lower $\delta^{44/40}\text{Ca}$ than pristine melting residues, but the difference is small except for some samples with very low CaO and Al_2O_3 (≤ 1 wt.%). The $\delta^{44/40}\text{Ca}$ are correlated with Ca/Al in the Obn suite, but not for xenoliths from the Udachnaya kimberlite (small rhombs, Kang et al., 2017).

the leachate and $0.70 \pm 0.12\text{‰}$ for the residue of Obn 22-13, and $0.83 \pm 0.06\text{‰}$ for the leachate and $0.81 \pm 0.08\text{‰}$ for the residue of Obn 39-13. To sum up, the $\delta^{44/40}\text{Ca}$ values of the leachates and residues are essentially the same within analytical uncertainty suggesting that the metasomatic carbonates do not differ significantly in $\delta^{44/40}\text{Ca}$ from the host rock.

5. DISCUSSION

5.1. $\delta^{44/40}\text{Ca}$ in refractory, melt-depleted peridotite mantle

The Obn and Tariat peridotite xenoliths are fragments of the lithospheric mantle, which is believed to form from the asthenosphere either by conductive cooling or, most commonly, by additions of solidified melt extraction residues. Kang et al. (2017) estimated the $\delta^{44/40}\text{Ca}$ value in the bulk silicate Earth (BSE; $0.94 \pm 0.05\text{‰}$) from data for fertile off-craton lherzolite xenoliths, which experienced no or only very low degrees of partial melting, and have major oxide compositions (MgO , Al_2O_3 , CaO etc.) similar to those of the primitive mantle (PM). They further argued that $\delta^{44/40}\text{Ca}$ values for refractory peridotites (formed by high degrees of melt extraction from fertile mantle) are somewhat higher ($1.06 \pm 0.04\text{‰}$) if they are not significantly affected by post-melting metasomatism (Fig. 4).

The $\delta^{44/40}\text{Ca}$ values of the four melt-depleted peridotites from Mongolia (0.96 – 1.12‰) follow the trends defined by the samples reported by Kang et al. (2017) in plots vs. Al_2O_3 and CaO (Fig. 4a and b). Their averages ($1.04 \pm 0.08\text{‰}$ for all four, and $1.10 \pm 0.03\text{‰}$ for two most refractory samples with the lowest Al and Ca) are consistent with the conclusion of Kang et al. (2017) on the effects of melting on $\delta^{44/40}\text{Ca}$ in residues. Combining the data on peridotites with $\text{Al}_2\text{O}_3 < 2$ wt.% from the study of Kang et al. (2017) and this work yields an average of $1.08 \pm 0.03\text{‰}$ for refractory mantle, i.e. $\sim 0.14\text{‰}$ heavier than the BSE estimate.

The Obn peridotites studied here, however, are neither fertile mantle samples, nor pristine melting residues because their modal and chemical compositions have been strongly affected by melt metasomatism (Ionov et al., 2018b). The dunites (low-Ca-Al peridotites) appear to be melt channel materials formed by reaction of peridotites with mafic melts, while the ubiquitously high CaO and Ca/Al (Fig. 3b and c), as well as occasional carbonates and late-stage cpx, in the remainder of the peridotite suite suggest important Ca input, most likely by carbonate-rich melts. The effects of melt extraction on Ca isotope ratios in these samples must have been obscured by the later processes.

5.2. Ca-isotope signatures of mantle metasomatism

5.2.1. $\delta^{44/40}\text{Ca}$ in carbonate-bearing xenoliths

The effects of carbonatite metasomatism on $\delta^{44/40}\text{Ca}$ of mantle peridotites are examined here directly using analyses of natural carbonate-bearing xenoliths, which are very rare worldwide (e.g. Ionov et al., 1993). The precursors of Ca-rich, low-Al (0.4 – 1.9 wt.% Al_2O_3) Obn peridotites were refractory melting residues, possibly akin to melt-depleted

Table 3
The Ca isotope composition of leachate, residue and calculated bulk rock.

Sa. No.		Ca fraction	$\delta^{44/42}\text{Ca}$ relative to ICPI	2SD	$\delta^{44/40}\text{Ca}$ relative to SRM 915a	$\delta^{44/40}\text{Ca}$ relative to SRM 915b	2SD	n
Obn-8/13	Leachate	0.18	0.05	0.00	0.82	0.12	0.01	3
	Residue	0.83	0.06	0.03	0.84	0.14	0.06	3
	Calculated bulk	1.00			0.83	0.13	0.06	3
Obn-22/13	Leachate	0.75	0.06	0.02	0.84	0.14	0.04	3
	Residue	0.25	−0.01	0.06	0.70	0.00	0.12	3
	Calculated bulk	1.00			0.81	0.11	0.12	3
Obn-39/13	Leachate	0.75	0.05	0.03	0.83	0.13	0.06	3
	Residue	0.25	0.02	0.03	0.77	0.07	0.06	3
	Calculated bulk	1.00			0.81	0.11	0.08	3

ICPI, in-house Ca isotope standard (see text).

Tariat peridotites (Section 5.1), assuming that Al concentrations are not affected by the metasomatism. The $\delta^{44/40}\text{Ca}$ values of WR Obn xenoliths containing metasomatic carbonates (0.74–0.88‰) are consistently lower (by 0.2–0.3‰) than for their likely residual protoliths (1.08 ± 0.03‰ as discussed in the previous section). It follows that the metasomatism of the Obn peridotites by carbonate-rich media reduced $\delta^{44/40}\text{Ca}$ values, but the Ca isotope change is moderate.

Mass balance estimates using modal abundances (Table 1) and observed Ca concentrations in minerals (Ionov et al., 2018b) show that calcite hosts 75–85% of Ca in these rocks. The fact that $\delta^{44/40}\text{Ca}$ values are similar for acid-leachates (i.e. dissolved carbonates) and leaching residues (silicates) for all the samples may indicate that the carbonates are close to isotope equilibrium with Ca-bearing silicates (mainly garnet and cpx) in the host peridotites. This must be the case for garnet, which is texturally equilibrated with calcite in pockets formed by reaction of metasomatic liquids with opx and spinel (Fig. 2c and d). In contrast, cpx in these rocks only occurs outside the calcite- and garnet-bearing pockets and may have existed before their formation. Trace element data (Ionov et al., 2018b) suggest that the cpx may not be fully equilibrated with the garnet in the metasomatic pockets.

Another xenolith strongly reworked by the carbonatite-type metasomatism is Obn 24-13, in which much of the opx is replaced with cpx-phlogopite pockets (Fig. 2a; Ionov et al., 2018b). This sample has the lowest $\delta^{44/40}\text{Ca}$ (0.56‰) for this study, i.e. ≥0.2‰ lower than for the carbonate-bearing Obn peridotites and ~0.5‰ lower than for unmetasomatized Tariat peridotites. This peridotite contains very little Al_2O_3 (0.41 wt.%) and has a very high Ca/Al of 8, suggesting that its Ca budget is dominated by metasomatic Ca input (Fig. 3c).

It appears that, in general, the greatest metasomatism-induced Ca isotope offsets in the Obn suite are for rocks initially very low in Ca that experienced high Ca additions relative to their Ca contents before the metasomatism, and developed high Ca/Al ratios. The Obn suite defines a negative Ca/Al vs. $\delta^{44/40}\text{Ca}$ trend (Fig. 4c), which remains significant (linear correlation coefficients of 0.4–0.7) also without the two samples with the highest Ca/Al (5.9 and 8.0). Thus,

assuming that all the Ca-rich, low-Al Obn peridotites were metasomatized by the same liquid the $\delta^{44/40}\text{Ca}$ of such a liquid could be close to 0.5‰, like in Obn 24-13. Alternatively, xenolith Obn 24-13 may have been metasomatized by a batch of Ca-rich liquid with lower $\delta^{44/40}\text{Ca}$ than for other Obn peridotites. It is also likely that the $\delta^{44/40}\text{Ca}$ in the metasomatic media evolved as they percolated through the residual mantle with higher $\delta^{44/40}\text{Ca}$.

We infer that the metasomatism of the type that produced the carbonate-bearing Obn xenoliths tends to decrease the $\delta^{44/40}\text{Ca}$ values of residual mantle rocks, but its effects are usually limited (≤0.3‰) even in cases of strong Ca enrichments and apparent Ca isotope equilibration between the metasomatic media and the reworked peridotites.

5.2.2. Ca isotope signatures of “carbonatite” vs. “silicate” metasomatism

Kang et al. (2017) reported $\delta^{44/40}\text{Ca}$ ranging from 0.25 to 0.96‰ for six harzburgites and low-cpx lherzolites with “carbonatite-type” metasomatism (inferred from WR and cpx REE patterns) from the Udachnaya kimberlite in the central Siberian craton and from Tariat (Fig. 1; Ionov et al., 2010; Doucet et al., 2012). They found the lowest $\delta^{44/40}\text{Ca}$ of 0.25‰ in a single sample extremely low in Al_2O_3 (0.09 wt.%) and with high Ca/Al (3.9), but other low- $\delta^{44/40}\text{Ca}$ (0.55–0.79‰) xenoliths from Kang et al. (2017) have both low CaO and low Ca/Al (Fig. 4b and c), unlike those in this study. Furthermore, Kang et al. (2017) reported $\delta^{44/40}\text{Ca}$ of 0.83–0.89‰ for three Ca-Al-rich lherzolites affected by “silicate-melt” metasomatism (Fig. 4), which overlap the $\delta^{44/40}\text{Ca}$ range for the carbonate-bearing Obn xenoliths.

The $\delta^{44/40}\text{Ca}$ range for eight out of nine metasomatized xenoliths from Kang et al. (2017) (0.55–0.96‰) is nearly the same as for the Obn xenoliths studied here apart from two unusual Obn peridotites (see next section) with high $\delta^{44/40}\text{Ca}$ (Fig. 4). In particular, the $\delta^{44/40}\text{Ca}$ range in the Udachnaya and Tariat xenoliths presumably affected by the silicate-melt metasomatism (0.83–0.89‰) overlaps the $\delta^{44/40}\text{Ca}$ range in the carbonate-bearing and other Ca-rich Obn xenoliths of this study. We conclude that $\delta^{44/40}\text{Ca}$ cannot be used to robustly distinguish between “carbonatite”

and “silicate” metasomatism. It appears, however, that the lowest $\delta^{44/40}\text{Ca}$ in the lithospheric mantle may be found mainly in the most refractory, low-Al peridotites.

5.3. Peridotites with high $\delta^{44/40}\text{Ca}$

The $\delta^{44/40}\text{Ca}$ of 1.22 and 1.38‰ in two Obn xenoliths are enigmatic because they are too high to be attributed either to melt extraction from fertile mantle (Section 5.1) or to reaction with the same Ca-rich metasomatic media that affected the other Obn xenoliths (which have lower $\delta^{44/40}\text{Ca}$). Metasomatized Tariat xenoliths have lower $\delta^{44/40}\text{Ca}$ as well (Section 5.2.2). Alternative explanations could take into account the evidence that both anomalous Obn samples were affected by silicate melt percolation. Fig. 2b shows that peridotite Obn 68-13 was sampled close (1–2 cm) to a websterite vein, composed of opx and cpx with minor olivine and spinel. Fine-grained spinel websterite veins with gradational contacts in this and other Obn xenoliths formed shortly before the kimberlite eruption because long residence in the mantle leads to recrystallization to more coarse and texturally equilibrated rocks (Ionov et al., 2018b). Furthermore, the absence of sharp contacts with host peridotites excludes an origin by intrusion of the kimberlite magma that carried the xenoliths.

It is conceivable that the silicate liquid, which formed the pyroxenite vein, had a high $\delta^{44/40}\text{Ca}$ and conveyed this Ca-isotope signature to the host peridotite by infiltration. This hypothesis cannot be tested directly because we have no Ca-isotope data on the vein, but it does not appear likely. First, $\delta^{44/40}\text{Ca}$ values for erupted continental and oceanic basaltic magmas are $<1.2\text{‰}$ (e.g. Zhu et al., 2018). Second, the WR trace element pattern of Obn 68-13 is very similar to that of other Obn peridotites in this study (Ionov et al., 2018b) that show much lower $\delta^{44/40}\text{Ca}$. Finally, two pyroxenites analyzed in this study, including another fine-grained websterite, show lower $\delta^{44/40}\text{Ca}$ (0.74–0.93‰; Table 2) further arguing against a source liquid with an anomalously high $\delta^{44/40}\text{Ca}$.

A detailed study, with analyses of the vein and of the host peridotites at different distances from the vein, is needed to examine the high $\delta^{44/40}\text{Ca}$ in Obn 68-13. However, a viable alternative could be diffusion-driven kinetic fractionation of Ca isotopes at the melt-rock boundary, similar to that invoked to explain experimentally produced $\delta^{44/40}\text{Ca}$ fractionation of 6‰ at the interface of molten basalt and rhyolite (Richter et al., 2003) or anomalous Cr isotope ratios in veined Tariat xenoliths (Xia et al., 2017). A diffusion-controlled process may have also enriched dunite Obn 59-13 (likely of melt-channel origin) in heavy Ca isotopes.

Kinetic fractionation of metal stable isotopes during melt-rock reaction and melt percolation was earlier invoked for Li, Fe, Mg (Weyer and Ionov, 2007; Pogge von Strandmann et al., 2011; Teng et al., 2011; Xiao et al., 2013; Foden et al., 2018; Wu et al., 2018) and other elements. Evidence for diffusion-controlled Ca isotope fractionation has been previously reported for a suite of peridotite xenoliths from North China that show anomalously low $\delta^{44/40}\text{Ca}$ (–0.08 to 0.92‰) and $\delta^{57/54}\text{Fe}$ (Zhao

et al., 2017). Variable, but generally low, Mg# in those xenoliths are attributed to percolation of evolved basaltic liquids and possibly compositional effects of Ca isotopic fractionation between co-existing cpx and opx, supported by numeric modeling (Huang et al., 2010; Wang et al., 2017). Mass balance considerations suggest that if such a process produces a low- $\delta^{44/40}\text{Ca}$ component, it should also produce a complementary high- $\delta^{44/40}\text{Ca}$ component, which might explain the high- $\delta^{44/40}\text{Ca}$ values in the two Obn samples.

5.4. Ca isotopes as tracers of Ca recycling

Mantle metasomatism by carbonatite and carbonate-rich silicate liquids extracted from subducted slabs that contain sedimentary carbonates has been repeatedly invoked for lithospheric erosion and reworking of the mantle lithosphere, in particular beneath the North China craton (e.g. Chen et al., 2018). Our study, however, finds no coherent and significant Ca isotope variations in mantle xenoliths that could be seen as robust evidence either for carbonatite metasomatism or links to subduction-related materials and tectonic settings.

Kang et al. (2017) speculated that low $\delta^{44/40}\text{Ca}$ values in metasomatized mantle xenoliths may be linked to recycled crustal materials because the Ca isotope compositions of sedimentary carbonates are highly heterogeneous and many of these rocks have lower $\delta^{44/40}\text{Ca}$ than BSE estimates (e.g. Fantle and Tipper, 2014; Griffith et al., 2015; Husson et al., 2015; Farkaš et al., 2016). In particular, Fantle and Tipper (2014) reported a $\delta^{44/40}\text{Ca}$ range from –1.1 to 1.8‰ for 1301 carbonate rocks (with 95% of data from –0.2 to +1.3‰) and a mean of $0.60 \pm 0.02\text{‰}$, which is lower than the mean ($0.94 \pm 0.04\text{‰}$) they obtained for 153 silicate rocks and minerals. Earlier, Huang S. et al. (2011) attributed $\sim 0.3\text{‰}$ variation in $\delta^{44/40}\text{Ca}$ for 11 Hawaiian tholeiites (0.75–1.05‰) to addition of up to 4% of hypothetical recycled marine carbonates with $\delta^{44/40}\text{Ca}$ of 0.2‰ to a plume component with $\delta^{44/40}\text{Ca}$ of 1.05‰.

In contrast, a more recent data compilation for 505 Precambrian (0.54–3.0 Ga) carbonates (Blättler and Higgins, 2017) yielded an average $\delta^{44/40}\text{Ca}$ of 0.94‰ and showed that the means for samples from 12 time intervals with >10 analyses did not exhibit a persistent temporal trend. Blättler and Higgins (2017) argued that the mean of the available carbonate sediment dataset is indistinguishable from $\delta^{44/40}\text{Ca}$ estimates for the BSE within uncertainty. Blättler and Higgins (2017) also reported a $\delta^{44/40}\text{Ca}$ range of 0.5–1.3‰ for carbonate veins from a drilled section of 170 Ma altered oceanic crust, with the majority of the data between 0.88 and 1.28‰. They noted that the average for veins from this and the majority of other drilled sites are higher than BSE estimates, which implies that alteration of oceanic crust may not produce low $\delta^{44/40}\text{Ca}$ values in subducted slabs.

Two aspects of the data in this study are consistent with the contention that sediment recycling and subduction of oceanic crust may not produce significant bulk changes in the Ca isotope composition of the mantle. The first is that metasomatism does not appear to produce considerable

$\delta^{44/40}\text{Ca}$ shifts from the BSE value in the majority of studied mantle peridotites. This is expected if the mean $\delta^{44/40}\text{Ca}$ of recycled crustal materials is similar to that of the convecting mantle. The second argument is the lack of clear differences in the $\delta^{44/40}\text{Ca}$ values of mantle xenoliths affected by “carbonatite” vs. “silicate” mantle metasomatism (Section 5.2.2). The opposite should be observed if carbonatite liquids are derived from the recycling of sedimentary carbonates with $\delta^{44/40}\text{Ca}$ distinct from those of mafic silicate melts, which are thought to be derived by low-degree melting and fractionation in upwelling deep mantle.

It is difficult, however, to assess how spatially heterogeneous and extreme could be the $\delta^{44/40}\text{Ca}$ values of subducted carbonate sediments and their derivatives on a local or a regional scale. Blättler and Higgins (2017) reported standard deviations ranging from 0.03 to 0.27‰ for mean $\delta^{44/40}\text{Ca}$ values of individual sections/formations (with ≥ 10 analyses) of their carbonate dataset, which may reflect Ca isotope variability within the formations. Mingling of fluids expelled from different parts of subducted slab (e.g. various sediments and altered oceanic crust) may further reduce Ca isotope variability in the metasomatic media injected to the mantle. Although one cannot rule out that recycling of sedimentary units with anomalous $\delta^{44/40}\text{Ca}$ values could locally introduce to the mantle carbonate-rich fluids or liquids that differ from the BSE estimate ($0.94 \pm 0.05\%$) by $>0.5\%$ (highest 2SD values for individual formations reported by Blättler and Higgins, 2017), such cases may be rare.

This contention is supported by the limited currently available Ca-isotope data on mantle rocks. The $\delta^{44/40}\text{Ca}$ values in carbonate-bearing Obn xenoliths are just 0.10–0.15‰ lower than the BSE estimate. Only one out of 50 samples from six eruption centers reported here and by Kang et al. (2017) deviates by $>0.5\%$ from the BSE value. This speaks for limited Ca isotope variability in liquids expelled from subducted slabs, and/or effective homogenization of their compositions on the way to the mantle domains studied so far. Stronger $\delta^{44/40}\text{Ca}$ deviations by metasomatism cannot be ruled out at present, but may be rare; in some cases they may be due to kinetic isotope fractionation rather than exotic source compositions (Section 5.3). Overall, it appears that Ca isotopes have little use as a tracer of carbonate recycling.

Chen et al. (2018) reported a $\delta^{44/40}\text{Ca}$ range of 0.8–1.2‰ in pyroxenes (cpx and opx) from metasomatized peridotite xenoliths at Fanshi in NE China. This range extends to higher values than for the peridotites reported in this study and the literature (Kang et al., 2017; Zhao et al., 2017). Chen et al. (2018) contended that the heavy Ca isotope compositions are inconsistent with low $\delta^{44/40}\text{Ca}$ in carbonated sediments from the Paleo-Asian ocean and attributed the high $\delta^{44/40}\text{Ca}$ to Ca isotope fractionation during subduction of carbonated sediments. The latter argument, however, may be at odds with their conclusion that Ca isotopes can be used to detect recycled crustal materials in the mantle.

To sum up, our data show no clear evidence that subduction and recycling of surface carbonates were responsible for mantle metasomatism and lithospheric erosion beneath Obnazhennaya. Overall, we see no evidence that Ca isotopes are robust and unequivocal tracers of recycling of surface carbonates to the mantle. It appears that although the Ca isotope range in some sedimentary carbonate suites is broad, their global, regional and temporal averages may not be very different from $\delta^{44/40}\text{Ca}$ in the BSE (Blättler and Higgins, 2017) and the most common mantle peridotites. It is also possible that local Ca isotope heterogeneities in subducted rocks are leveled out during the extraction of carbonate-rich fluids from the slab, and mingling and transport of the fluids/melts to the mantle lithosphere. Finally, while fluids released from subducted slabs impact the mantle wedge, the subducted sediments are ultimately stored in the deep mantle where they contribute to plume sources (e.g. Zeng et al., 2010). In such a case, Ca isotope signatures of melts and fluids generated by recent subduction events may be similar to those of plume-related magmatism.

6. SUMMARY OF CONCLUSIONS

The scope and the origin of Ca isotope variations in the lithospheric mantle are examined using analyses of 22 mantle xenoliths, including the first data on carbonate-bearing mantle rocks, as well as literature results. The $\delta^{44/40}\text{Ca}$ range of $1.10 \pm 0.03\%$ determined for refractory, non-metasomatized off-craton peridotites is higher than the BSE estimate ($0.94 \pm 0.05\%$) based on fertile Iherzolites (Kang et al., 2017) due to isotope fractionation during melt extraction.

The $\delta^{44/40}\text{Ca}$ range for the majority of metasomatized peridotites from the Obnazhennaya kimberlite on the SE Siberian craton is narrow (0.74–0.97‰) and overlaps the BSE value. Bulk $\delta^{44/40}\text{Ca}$ in Obn peridotites containing metasomatic calcite ranges from 0.81 to 0.83‰, with similar values in acid-leachates (carbonates) and leaching residues. Metasomatism tends to decrease the $\delta^{44/40}\text{Ca}$ values of the affected mantle rocks, but the effects are usually limited ($\leq 0.3\%$). Peridotites that were refractory and Ca-poor before the metasomatism, and which received the greatest relative Ca input (seen as high Ca/Al) usually have the lowest $\delta^{44/40}\text{Ca}$.

We find no evidence that $\delta^{44/40}\text{Ca}$ can robustly distinguish between “carbonatite” and “silicate” metasomatism, or that recycling of crustal carbonates may greatly affect Ca isotope compositions in the global mantle. The latter may not be very different from the global mean $\delta^{44/40}\text{Ca}$ of subducted sedimentary carbonates implying that Ca isotopes have little use as a tracer of carbonate recycling. It is conceivable, however, that anomalous $\delta^{44/40}\text{Ca}$ values are produced locally by kinetic isotope fractionation during intrusion and percolation of melts in channels and host peridotites. Ca isotope signatures of melts and fluids generated by recent subduction events may be similar to those of plume-related magmatism containing sediments subducted long time ago.

ACKNOWLEDGEMENTS

DAI acknowledges the Chinese Academy of Sciences President's International Fellowship Initiative (PIFI) for Visiting Scientists in 2017–18 taken up at GIG (Guangzhou). AVG and OBO were supported by Russian Federation state assignment projects of IGM SB RAS and of DPMGI SB RAS. Stephen Romaniello and Gwyneth Gordon provided assistance with isotope analysis. We thank three anonymous reviewers for extensive comments that helped us to improve the manuscript, and Mark Rehkämper for valuable advice and efficient editorial handling.

REFERENCES

- Albarede F. and Beard B. (2004) Analytical methods for non-traditional isotopes. *Rev. Mineral. Geochem.* **55**, 113–152.
- Amini M., Eisenhauer A., Böhm F., Holmden C., Kreissig K., Hauff F. and Jochum K. P. (2009) Calcium isotopes ($\delta^{44/40}\text{Ca}$) in MPI-DING reference glasses, USGS rock powders and various rocks: evidence for Ca isotope fractionation in terrestrial silicates. *Geostand. Geoanal. Res.* **33**, 231–247.
- Amsellem E., Moynier F., Pringle E. A., Bouvier A., Chen H. and Day J. M. D. (2017) Testing the chondrule-rich accretion model for planetary embryos using calcium isotopes. *Earth Planet. Sci. Lett.* **469**, 75–83.
- Blättler C. L. and Higgins J. A. (2017) Testing Urey's carbonate–silicate cycle using the calcium isotopic composition of sedimentary carbonates. *Earth Planet. Sci. Lett.* **479**, 241–251.
- Chen C., Liu Y., Feng L., Foley S. F., Zhou L., Ducea M. N. and Hu Z. (2018) Calcium isotope evidence for subduction-enriched lithospheric mantle under the northern North China Craton. *Geochim. Cosmochim. Acta* **238**, 55–67.
- Doucet L. S., Ionov D. A., Golovin A. V. and Pokhilenko N. P. (2012) Depth, degrees and tectonic settings of mantle melting during craton formation: inferences from major and trace element compositions of spinel harzburgite xenoliths from the Udachnaya kimberlite, central Siberia. *Earth Planet. Sci. Lett.* **359–360**, 206–218.
- Fantle M. S. and Tipper E. T. (2014) Calcium isotopes in the global biogeochemical Ca cycle: implications for development of a Ca isotope proxy. *Earth-Sci. Rev.* **129**, 148–177.
- Farkaš J., Frýda J. and Holmden C. (2016) Calcium isotope constraints on the marine carbon cycle and CaCO_3 deposition during the late Silurian (Ludfordian) positive $\delta^{13}\text{C}$ excursion. *Earth Planet. Sci. Lett.* **451**, 31–40.
- Feng L. P., Zhou L., Yang L., DePaolo D. J., Tong S. Y., Liu Y. S., Owens T. L. and Gao S. (2016) Calcium isotopic compositions of sixteen USGS reference materials. *Geostand. Geoanal. Res.* **41**, 93–106.
- Foden J., Sossi P. A. and Nebel O. (2018) Controls on the iron isotopic composition of global arc magmas. *Earth Planet. Sci. Lett.* **494**, 190–201.
- Griffith E. M., Fantle M. S., Eisenhauer A., Paytan A. and Bullen T. D. (2015) Effects of ocean acidification on the marine calcium isotope record at the Paleocene-Eocene Thermal Maximum. *Earth Planet. Sci. Lett.* **419**, 81–92.
- He Y., Wang Y., Zhu C., Huang S. and Li S. (2016) Mass-independent and mass-dependent Ca isotopic compositions of thirteen geological reference materials measured by thermal ionisation mass spectrometry. *Geostand. Geoanal. Res.* **41**, 283–302.
- Heuser A., Eisenhauer A., Gussone N., Bock B., Hansen B. T. and Nägler T. F. (2002) Measurement of calcium isotopes ($\delta^{44}\text{Ca}$) using a multicollector TIMS technique. *Int. J. Mass Spectrom.* **220**, 385–397.
- Huang S., Farkaš J. and Jacobsen S. B. (2010) Calcium isotopic fractionation between clinopyroxene and orthopyroxene from mantle peridotites. *Earth Planet. Sci. Lett.* **292**, 337–344.
- Huang F., Zhang Z., Lundstrom C. C. and Zhi X. (2011a) Iron and magnesium isotopic compositions of peridotite xenoliths from Eastern China. *Geochim. Cosmochim. Acta* **75**, 3318–3334.
- Huang S., Farkaš J. and Jacobsen S. B. (2011b) Stable calcium isotopic compositions of Hawaiian shield lavas: evidence for recycling of ancient marine carbonates into the mantle. *Geochim. Cosmochim. Acta* **75**, 4987–4997.
- Husson J. M., Higgins J. A., Maloof A. C. and Schoene B. (2015) Ca and Mg isotope constraints on the origin of Earth's deepest $\delta^{13}\text{C}$ excursion. *Geochim. Cosmochim. Acta* **160**, 243–266.
- Ionov D. A. (2007) Compositional variations and heterogeneity in fertile lithospheric mantle: peridotite xenoliths in basalts from Tariat, Mongolia. *Contrib. Mineral. Petrol.* **154**, 455–477.
- Ionov D. A., Dupuy C., O'Reilly S. Y., Kopylova M. G. and Genshaft Y. S. (1993) Carbonated peridotite xenoliths from Spitsbergen: implications for trace element signature of mantle carbonate metasomatism. *Earth Planet. Sci. Lett.* **119**, 283–297.
- Ionov D. A., Doucet L. S. and Ashchepkov I. V. (2010) Composition of the lithospheric mantle in the Siberian craton: new constraints from fresh peridotites in the Udachnaya-East kimberlite. *J. Petrol.* **51**, 2177–2210.
- Ionov D. A., Carlson R. W., Doucet L. S., Golovin A. V. and Oleinikov O. B. (2015) The age and history of the lithospheric mantle of the Siberian craton: Re–Os and PGE study of peridotite xenoliths from the Obnazhennaya kimberlite. *Earth Planet. Sci. Lett.* **428**, 108–119.
- Ionov D. A., Doucet L. S., Carlson R. W., Golovin A. V. and Oleinikov O. B. (2018a) Lost in interpretation: facts and misconceptions about the mantle of the Siberian craton. A comment on: “Composition of the lithospheric mantle in the northern part of Siberian craton: constraints from peridotites in the Obnazhennaya kimberlite” by Sun et al. (2017). *Lithos* **314–315**, 683–687.
- Ionov D. A., Doucet L. S., Xu Y., Golovin A. V. and Oleinikov O. B. (2018b) Reworking of Archean mantle in the NE Siberian craton by carbonatite and silicate melt metasomatism: evidence from a carbonate-bearing, dunite-to-websterite xenolith suite from the Obnazhennaya kimberlite. *Geochim. Cosmochim. Acta* **224**, 132–153.
- Ionov D. A. and Hofmann A. W. (1995) Nb-Ta-rich mantle amphiboles and micas: implications for subduction-related metasomatic trace element fractionations. *Earth Planet. Sci. Lett.* **131**, 341–356.
- Ionov D. A. and Hofmann A. W. (2007) Depth of formation of sub-continental off-craton peridotites. *Earth Planet. Sci. Lett.* **261**, 620–634.
- Kang J.-T., Zhu H.-L., Liu Y.-F., Liu F., Wu F., Hao Y.-T., Zhi X.-C., Zhang Z.-F. and Huang F. (2016) Calcium isotopic composition of mantle xenoliths and minerals from Eastern China. *Geochim. Cosmochim. Acta* **174**, 335–344.
- Kang J.-T., Ionov D. A., Liu F., Zhang C.-L., Golovin A. V., Qin L.-P., Zhang Z.-F. and Huang F. (2017) Calcium isotopic fractionation in mantle peridotites by melting and metasomatism and Ca isotope composition of the Bulk Silicate Earth. *Earth Planet. Sci. Lett.* **474**, 128–137.
- Liu F., Zhu H. L., Li X., Wang G. Q. and Zhang Z. F. (2017) Calcium isotopic fractionation and compositions of geochemical reference materials. *Geostand. Geoanal. Res.* **41**, 675–688.
- McDonough W. F. and Sun S.-S. (1995) The composition of the Earth. *Chem. Geol.* **120**, 223–253.
- Palme H. and Nickel K. G. (1985) Ca/Al ratio and composition of the Earth's mantle. *Geochim. Cosmochim. Acta* **49**, 2123–2132.

- Pogge von Strandmann P. A. E., Elliott T., Marschall H. R., Coath C., Lai Y.-J., Jeffcoate A. and Ionov D. A. (2011) Variations of Li and Mg isotope ratios in bulk chondrites and mantle xenoliths. *Geochim. Cosmochim. Acta* **75**, 5247–5268.
- Richter F. M., Davis A. M., DePaolo D. J. and Watson E. B. (2003) Isotope fractionation by chemical diffusion between molten basalt and rhyolite. *Geochim. Cosmochim. Acta* **67**, 3905.
- Romaniello S. J., Field M. P., Smith H. B., Gordon G. W., Kim M. H. and Anbar A. D. (2015) Fully automated chromatographic purification of Sr and Ca for isotopic analysis. *J. Analyt. Atom. Spectrom.* **30**, 1906–1912.
- Tappe S., Romer R. L., Stracke A., Steinfeld A., Smart K. A., Muehlenbachs K. and Torsvik T. H. (2017) Sources and mobility of carbonate melts beneath cratons, with implications for deep carbon cycling, metasomatism and rift initiation. *Earth Planet. Sci. Lett.* **466**, 152–167.
- Teng F.-Z., Dauphas N., Helz R. T., Gao S. and Huang S. (2011) Diffusion-driven magnesium and iron isotope fractionation in Hawaiian olivine. *Earth Planet. Sci. Lett.* **308**, 317–324.
- Valdes M. C., Moreira M., Foriel J. and Moynier F. (2014) The nature of Earth's building blocks as revealed by calcium isotopes. *Earth Planet. Sci. Lett.* **394**, 135–145.
- Wang Z.-Z., Liu S.-A., Ke S., Liu Y.-C. and Li S.-G. (2016) Magnesium isotopic heterogeneity across the cratonic lithosphere in eastern China and its origins. *Earth Planet. Sci. Lett.* **451**, 77–88.
- Wang W., Zhou C., Qin T., Kang J.-T., Huang S., Wu Z. and Huang F. (2017) Effect of Ca content on equilibrium Ca isotope fractionation between orthopyroxene and clinopyroxene. *Geochim. Cosmochim. Acta* **219**, 44–56.
- Weyer S. and Ionov D. A. (2007) Partial melting and melt percolation in the mantle: the message from Fe isotopes. *Earth Planet. Sci. Lett.* **259**, 119–133.
- Wu H., He Y., Teng F.-Z., Ke S., Hou Z. and Li S. (2018) Diffusion-driven magnesium and iron isotope fractionation at a gabbro-granite boundary. *Geochim. Cosmochim. Acta* **222**, 671–684.
- Xia J., Qin L., Shen J., Carlson R. W., Ionov D. A. and Mock T. D. (2017) Chromium isotope heterogeneity in the mantle. *Earth Planet. Sci. Lett.* **464**, 103–115.
- Xiao Y., Teng F.-Z., Zhang H.-F. and Yang W. (2013) Large magnesium isotope fractionation in peridotite xenoliths from eastern North China craton: product of melt–rock interaction. *Geochim. Cosmochim. Acta* **115**, 241–261.
- Xu Y. (2002) Evidence for crustal components in the mantle and constraints on crustal recycling mechanisms: pyroxenite xenoliths from Hannuoba, North China. *Chem. Geol.* **182**, 301–322.
- Young E. D., Galy A. and Nagahara H. (2002) Kinetic and equilibrium mass-dependent isotope fractionation laws in nature and their geochemical and cosmochemical significance. *Geochim. Cosmochim. Acta* **66**, 1095–1104.
- Zeng G., Chen L.-H., Xu X.-S., Jiang S.-Y. and Hofmann A. W. (2010) Carbonated mantle sources for Cenozoic intra-plate alkaline basalts in Shandong, North China. *Chem. Geol.* **273**, 35–45.
- Zhao X., Zhang Z., Huang S., Liu Y., Li X. and Zhang H. (2017) Coupled extremely light Ca and Fe isotopes in peridotites. *Geochim. Cosmochim. Acta* **208**, 368–380.
- Zhu H., Liu F., Li X., Wang G., Zhang Z. and Sun W. (2018) Calcium isotopic compositions of normal mid-ocean ridge basalts from the southern Juan de Fuca Ridge. *J. Geophys. Res.: Solid Earth* **123**, 1303–1313.

Associate editor: Mark Rehkamper